Nonuniform photonic crystal taper for high-efficiency mode coupling

E. H. Khoo, A. Q. Liu, and J. H. Wu

School of Electrical and Electronic Engineering,
Nanyang Technological University, Nanyang Avenue, Singapore 639798
eaqliu@ntu.edu.sg

Abstract: A nonuniform-shape photonic crystal taper integrated with a single-mode optical fiber and a photonic crystal waveguide for high-efficiency mode coupling is presented. The curvature of the tapering section is varied by the parameter α. For values of α set to 2 and 0.5, concave and convex tapers are obtained, respectively. Numerical calculations yield an average coupling efficiency greater than 97% at a short taper length of 20.52 μm for the convex-shape taper. Subsequently, the value of the parameter α is varied for investigating the effects of curvature on coupling efficiency and compactness of different types of taper.

OCIS codes: (130.0130) Integrated Optics; (230.7380) Waveguides, channeled; (250.5300) Photonic integrated circuits.

References and links

1. J. D. Joannopoulos, R. D. Meade, and J. N. Winn, *Photonic Crystals: Molding the Flow of Light* (Princeton U. Press, 1995).
2. S. Fan, P. R. Villeneuve, J. D. Joannopoulos, and H. A. Haus, "Channel drop filters in photonic crystals," Opt. Express **3**, 4–11 (1998) http://www.opticsexpress.org/abstract.cfm?URI=OPEX-3-1-4.
3. D. Falco, C. Conti, and C. G. Someda, "Coupling and decoupling of electromagnetic waves in parallel 2-D photonic crystal waveguides," IEEE J. Quantum Electron. **38**, 47–53 (2002).
4. J. H. Wu, L. K. Ang, A. Q. Liu, H. G. Teo, and C. Lu, "Tunable high Q photonic bandgap Fabry–Perot resonator," J. Opt. Soc. Am. B **22**, 1770–1777 (2005).
5. S. G. Johnson, P. R. Villeneuve, S. H. Fan, and J. D. Joannopoulos, "Linear waveguide in photonic crystal slab," Phys. Rev. B **62**, 8212–8222 (2000).
6. D. Tailaert, W. Bogaerts, P. Bienstman, T. Krauss, P. V. Daele, I. Moerman, S. Verstuyft, K. D. Mesel, and R. Baets, "An out-of plane grating coupler for efficient butt coupling between compact planar waveguides and single mode fibres," IEEE J. Quantum Electron. **38**, 949–954 (2002).
7. P. E. Barclay, K. Srinivasan, M. Borselli, and O. Painter, "Efficient input and output fiber coupling to a photonic crystal waveguide," Opt. Lett. **29**, 697–699 (2004).
8. D. W. Prather, J. Murakowski, S. Shi, S. Venkataraman, C. Chen, and D. Pustai, "High-efficiency coupling structure for a single-line-defect photonic crystal waveguide," Opt. Lett. **27**, 1601–1603 (2002).
9. A. Mekis and J. D. Joannopoulos, "Tapered couplers for efficient interfacing between dielectric and photonic crystal waveguides," J. Lightwave Technol. **19**, 861–865 (2001).
10. Ph. Lalanne and A. Talneau, "Modal conversion with artificial materials for photonic-crystal waveguides," Opt. Express **10**, 354–359 (2002) http://www.opticsexpress.org/abstract.cfm?URI=OPEX-10-8-354.
11. M. Palamaru and Ph. Lalanne, "Photonic crystal waveguides: out-of-plane losses and adiabatic mode conversion," Appl. Phys. Lett. **78**, 1466–1468 (2001).
12. T. D. Happ, M. Kamp, and A. Forchel, "Photonic crystal tapers for ultracompact mode conversion," Opt. Lett. **26**, 1102–1104 (2001).
13. P. Bienstman, S. Assefa, S. G. Johnson, J. D. Joannopoulos, G. S. Petrich, and L. A. Kolodziejski, "Taper structures for coupling into photonic crystal slab waveguide," J. Opt. Soc. Am. B **20**, 1817–1821 (2003).
14. P. Pottier, I. Ntakis, and R. M. De La Rue, "Photonic crystal continuous taper for low-loss direct coupling into photonic crystal channel waveguides and further device functionality," Opt. Commun. **223**, 339–347 (2003).
15. C. Wei, F. Groen, M. K. Smit, I. Moerman, P. V. Daele and R. Baets, "Integrated optical elliptic couplers: modeling, design, and applications," J. Lightwave Technol. **15**, 906–911 (1997).
16. C. C. Constantinou and R. C. Jones, "Path-integral analysis of arbitrarily tapered multimode, graded-index waveguide: the inverse-square-law and parabolic tapers," IEE Proceedings **139**, 365–375 (1992).
17. D. Marcuse, "Radiation losses of tapered dielectric slab waveguides," Bell Syst. Tech. J. **49,** 273–290 (1969).

#8561 - $15.00 USD Received 23 August 2005; revised 8 September 2005; accepted 12 September 2005

18. W. K. Burns and A. F. Milton, "Mode conversion in planar-dielectric separating waveguide," IEEE J. Quantum Electron. **11,** 32–39 (1975).
19. S. G. Johnson, P. Bienstman, M. A. Skorobogatiy, M. Ibanescu, E. Lidorikis and J. D. Joannopoulos, "Adiabatic theorem and continuous couple-mode theory for efficient taper transition" Phys. Rev. E **66**, 066608 (2002).
20. F. Sporleder and H. G. Unger, *Waveguide tapers transition and couplers* (IEE, 1979).
21. G. Tayeb and D. Maystre, "Rigorous theoretical study of finite-size two-dimensional photonic crystals doped by microcavities," J. Opt. Soc. Am. A **14**, 3323–3332 (1997).
22. J. Yonekura, M. Ikeda, and T. Baba, "Analysis of finite 2-D photonic crystals of columns and lightwave devices using the scattering matrix method," J. Lightwave Technol. **17**, 1500–1508 (1999).
23. G. O. Olaofe, "Scattering by two cylinders," Radio Sci. **5**, 1351–1360 (1970).
24. H. Benisty, "Modal analysis of optical guides with two-dimensional photonic band-gap boundaries," J. Appl. Phys. **79**, 7483–7492 (1996).

1. Introduction

Photonic crystals (PCs) have attracted much interest since the 1980s for their ability to control light propagation in all directions with the existence of a photonic bandgap. The most fascinating property of these crystals is the introduction of defects to manipulate light propagation. The photonic crystal waveguide (PCWG) is one such device that is carved out from a PC by the introduction of line defects to guide light from one location to another [1]. Light with a frequency within the photonic bandgap propagates along the linear defects because of the presence of localized modes in the photonic bandgap. This unique characteristic of the PCWG enables the transmission of a lightwave around abrupt, sharp bends, which cannot be achieved by classical waveguides. This unique characteristic has motivated many researchers to design PC devices such as filter and ADD–DROP multiplexers [2-4]—with the PCWG as a basic structure—for realization of photonic integrated circuits for application in communication systems. In this paper, we discuss the 2D PC, which shares many features with the 3D PC but with a simpler calculation algorithm and a more-stable fabrication process [5]. The structure consists of high-refractive-index dielectric rods in an air-medium structure. The idea and design that are discussed in this paper can also be applied generally to other structures to obtain similar results.

For the application of a photonic-integrated circuit in a communication network system, the dimension of PC devices will need to be scaled down to the sub-micro-range. This requirement has posed many challenges in design, fabrication process, and measurement. However, the greatest problem arises from coupling external light sources efficiently to the narrow PCWG. Direct butt coupling from light sources to the narrow PCWG is not possible as this difference in the modal cross-sectional area results in high coupling loss. A serious problem arises because insufficient light coupled into PC devices will hinder their functionality and reliability. To solve this problem, several methods of coupling have been implemented to couple light efficiently to the PCWG. They can be generally divided into two categories: vertical- and lateral-coupling methods. One vertical-coupling method uses grating-based devices [6] for coupling. Another vertical-coupling method uses free-space coupling from a tapered fiber to the PCWG [7]. Both methods are often subject to arguments because of their unreliability in coupling efficiently from the source to the PCWG. Therefore, researchers have turned to lateral coupling (in plane coupling) for higher reliability and higher coupling efficiency. For lateral coupling, more-intensive studies are carried out by assuming 2D PCWG. A parabolic mirror called J-coupler [8] is designed to focus light onto the entrance of the PCWG. Incoming light is reflected at the mirror and, due to the converging properties of the parabolic mirror, will focus at the entrance of the PCWG in order to be guided into the waveguide. Another method uses an external taper-coupler waveguide to bring light to the waveguide [9]. These methods of coupling have generally introduced radiation loss, which lowered the coupling efficiency. Besides, additional coupling devices means there are more potential loss spots, thus increasing losses. This in turn reduces the coupling efficiency of the coupling devices.

#8561 - $15.00 USD Received 23 August 2005; revised 8 September 2005; accepted 12 September 2005

PC tapers have been integrated with PCWGs for direct coupling between an optical source and a PCWG. This can be done by varying the size of the unit lattice to provide adiabatic mode conversion [10,11]. By way of the progressive variation of geometry, light traveling through the taper will experience adiabatic mode transformation. This method gives a high degree of freedom for design. However, it poses fabrication difficulty due to the different hole sizes and the need for very precise fabrication control and accuracy. It is also largely dependent on the geometry of the holes for adiabatic mode conversion of incident mode. The taper can also be introduced in its structural form to the coupling of light into the PCWG. It is implemented on the crystal structure by selectively removing holes to form the taper shape [12]. The taper device provides mode conversion laterally by virtue of its shape and can be used for direct mode conversion between a light source and a PCWG. It allows the design of a compact coupling structure but suffers from a serious setback of high radiation loss and back reflection at the uneven sidewall of the taper. To solve this problem, a linear PC taper [13,14] with a smooth sidewall has been designed to reduce the losses. The linear PC taper is created by distorting and shearing the crystal lattice.

The objective of this paper is motivated by the problems of optical fiber butt coupling to the PCWG. The aim is to design a nonuniform PC taper in the form of a smooth curve shape to obtain higher mode conversion and coupling efficiency to the narrow PCWG at a shorter taper length. Two complementary nonuniform shapes, concave and convex tapers [15,16], will be investigated and compared with the linear taper for compactness, low reflection loss, as well as higher coupling-efficiency improvement.

2. Taper structure of the waveguide

A tapered waveguide is an elongated guiding structure for electromagnetic wave transmission that gradually becomes narrower toward one end. Figure 1(top) shows the schematic layout of the linear tapered waveguide between two different cross-sectional waveguides. The cross-sectional mode distribution on the larger waveguide is “compressed” to the smaller mode distribution of the narrower waveguide by the virtue of the linear taper structure. In this section, the mode coupling mechanism in the tapering section will be discussed.

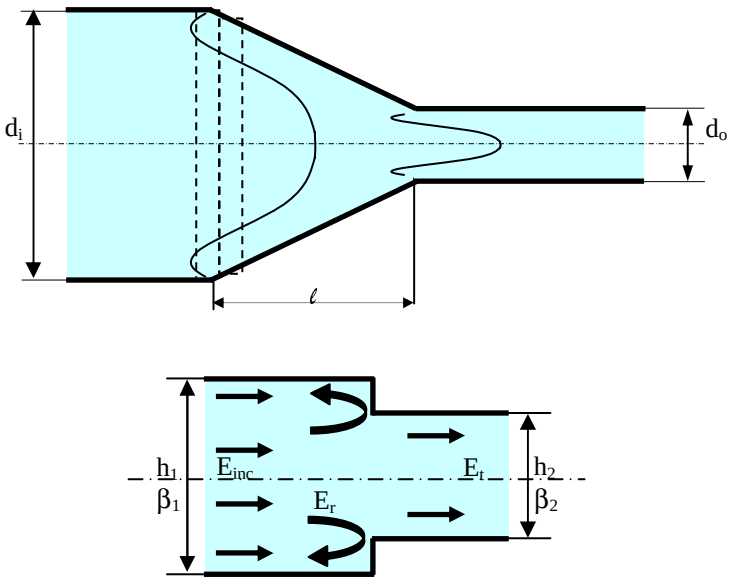

Fig. 1. *Top*: General layout of taper waveguide. *Bottom*: Diagram showing step analysis for mode conversion in a taper waveguide.

#8561 - $15.00 USD Received 23 August 2005; revised 8 September 2005; accepted 12 September 2005

The main function of the tapered waveguide is to provide low loss connections between waveguides with different cross-sectional areas. Possible sources of loss such as back reflection, intermodal coupling loss, radiation, and scattering loss arise as a result of the tapering of mode distribution between the source and the waveguide size. These losses are due to the change in the propagation constant of the taper, which in turn affects the mode-coupling efficiency of the taper. In this paper, the characteristic of the taper for effective mode coupling will be briefly analyzed using the step transition method.

The step transition method [17,18] divides the taper into many steps to account for the propagation constant change and hence loss analysis. As light travels through the taper, modal conversion will be performed to match the changes in the width of the waveguide. The half-width of the waveguide is related to the effective group index as

$$z(x) = \frac{m\lambda}{2\sqrt{n_{core}^2 - n_g^2}} \tag{1}$$

where m is the number of modes and n_{core} is the refractive index of the waveguide, which is air in this paper. λ is the propagating wavelength and n_g is the effective group index of the waveguide. The mode interaction between two steps is shown in Fig. 1(bottom).

For simplification, the case where both sides support only one mode is considered. The step on the left-hand side has a width of h_1, whereas the step on the right-hand side has a width of h_2. Due the difference in width of the waveguide, the incident light E_{inc} will experience a change in the propagation constant where most of the light will be transmitted to the step on the right, and the remaining will be reflected or radiated out. The determination of mode-coupling efficiency comes from minimizing the reflection of the light into the source or reducing radiation loss. Based on the boundary condition between the two steps, the approximated reflection coefficient is given as [18]

$$r = \left(\frac{\beta_1 - \beta_2}{\beta_1 + \beta_2}\right) exp(-i2\beta_1) \tag{2}$$

and the transmission coefficient is given as

$$c = 2\frac{\sqrt{\beta_1\beta_2}}{(\beta_1 + \beta_2)}\frac{I_{1,2}}{\sqrt{I_{1,1}I_{2,2}}} exp\left[-i(\beta_1 + \beta_2)\right] \tag{3}$$

where

$$I_{\alpha,\gamma} = \int E_\alpha E_\gamma dz \qquad \alpha,\gamma = 1,2 \tag{4}$$

and β_1 and β_2 are the propagation constants on the left-hand and right-hand steps, respectively. $I_{\alpha,\gamma}$ is the integral of the field overlap between the incident and transmitted field distribution.

Eqs. (2)–(4) are derived based on the simplification and approximation of a single-mode to single-mode transmittance. The main objective is to provide a simple analysis on the factors affecting the coupling efficiency for the tapering section. For real taper analysis, there are multimodes, and hence intermodal coupling between modes is observed as light propagates through the taper. Eqs. (2)–(4) have to be modified for the calculation of intermodal coupling between the fundamental mode and the higher-order modes. Readers can refer to Ref. [19] for more-precise calculation. For short tapers, the main loss mechanism is the reflection loss [20]. It arises due to the cutoff of the higher-order modes as the taper gets narrower. This problem can be solved by increasing the length of the taper to achieve slow tapering. As the length of the taper increases, light that propagates through the taper experiences adiabatic behavior, and high transmission is achieved. In this paper, the intermodal loss in the taper is assumed to be negligible compared with the reflection loss. The reflection loss can be minimized by altering the shape of the taper from linear to nonuniform. The nonuniform taper is designed by manipulating the crystal lattice of the PC, which will be discussed in Section 3.

#8561 - $15.00 USD Received 23 August 2005; revised 8 September 2005; accepted 12 September 2005

For a PC taper waveguide, the group index of the waveguide can be determined by taking the slope of the defect mode that is introduced in the bandgap region for the particular wavelength in the dispersion diagram. The group index is expressed as

$$n_g = c\left(\frac{\partial \omega}{\partial k}\right)^{-1} \tag{5}$$

This paper will relate the effect of taper slope (hence variation of the taper width) for high coupling efficiency. The number of modes in the taper waveguide is dependent on the width of the taper. For a converging taper (the width decreases along the taper), the number of mode also decreases along the taper. In the paper, the PCWG is a single-mode waveguide obtained through the removal of a row of rods in the Γ-X direction.

3. Nonuniform PC tapered waveguide

The curvature of the taper is obtained by lattice distortion of the regular crystal arrangement, as shown in Fig. 2. The equation of designing a taper with different curvature is expressed as

$$z = d_i + (d_i - d_o)\left[\left(1 - \frac{x}{l}\right)^{\alpha} - 1\right] \tag{6}$$

where the parameters, d_i and d_o are the input and output width of the taper, respectively. In this paper, d_i is 10 μm, which is approximately the mode diameter of a light pulse from a single-mode optical fiber. z and x are the coordinates of the rods to be placed for different taper shapes.

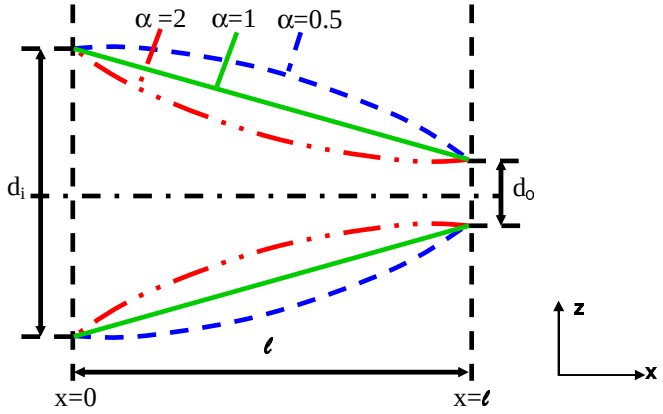

Fig. 2. Tapered-waveguide shapes for different values of α. For α = 1, the taper shape corresponds to the linear taper. For α = 2 and α = 0.5, the taper shape corresponds to concave and convex taper, respectively.

The width of PCWG is created by simply removing a row of rods from the PC lattice. Variables x and $z(x)$ are defined as the x-position and z-position of the rods with l as the total length of the taper. For square array arrangement, the x- and z-position of the rods will be multiples of the lattice constant. Based on Eq. (6), the designs of the nonuniform taper curve depend on the parameter α. When $\alpha = 1$, the taper is a linear taper structure. When other values of α are substituted, nonuniform-shape tapers are obtained. The values of $\alpha = 0.5$ and $\alpha = 2$ is investigated first to obtain two nonuniform tapers. Figure 2 shows the curvature of the taper with three values of α. When $\alpha = 2$, the taper is concave as the slope is decreasing toward the end of the taper. When $\alpha = 0.5$, a convex taper is obtained as the slope is increasing toward the end of the taper. The length of taper l is measured from the input end to the output end of the taper. By varying the length of the taper, the mode-conversion efficiency can be improved to increase the coupling efficiency.

#8561 - $15.00 USD Received 23 August 2005; revised 8 September 2005; accepted 12 September 2005

Based on Eq. (6), the taper shape is created by positioning the innermost row of rods that are defined by coordinates x and $z(x)$. The crystal is built in such a way that the vertical and horizontal lattice vectors are maintained at the lattice constant of a, shown in Fig. 3. In this paper, the light source that is incident from normal single-mode fiber is assumed to follow a Gaussian beam mode distribution. The collected field is then converted to power using the Poynting vector theorem. This output power is normalized with the incident power to obtain the normalized transmittance for different tapers.

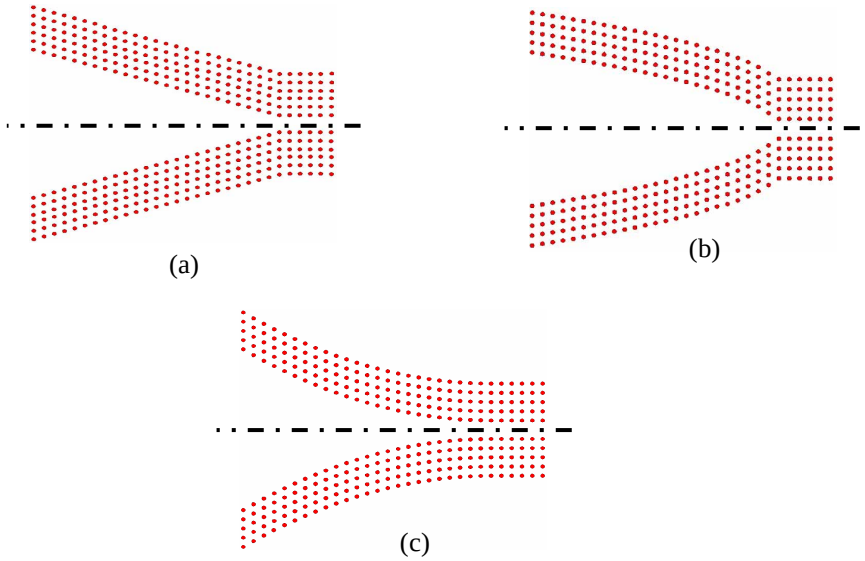

Fig. 3. Schematic layout of the PC taper: (a) linear; (b) convex; (c) concave.

4. Numerical method of PC

In this paper, the PC lattice consists of a square array of rods in a vacuum. The rods have a refractive index of $n = 3.45$, which is equivalent to silicon material. The crystal lattice has a filling ratio of $r/a = 0.2$, where r is the radius of the rod and a is the lattice constant. This ratio is used to obtain a large bandgap in TM polarization for rod configuration. The transverse magnetic (TM) polarization is defined to have the magnetic field in the x-z plane, the electric field perpendicular to the x-z plane, and vice versa for the TE polarization.

The scattering matrix method [21,22] is used in the simulation of the PC taper waveguide design. Compared with plane wave and finite difference method, the scattering matrix method is more efficient and accurate for obtaining transmission spectra. This is due to the high convergence rate with truncated series. Another special characteristic is that this method also allows arbitrary distribution of finite array for the calculation of transmission spectra, because it is dependent on the scattering position of the individual rods. This allows the placement of rods in such a position that they form different nonuniform taper curvatures for coupling.

The basic principle of the scattering-matrix method involves solving the scalar Helmholtz equation to obtain the scattering field of the periodic array and then summing them up to obtain the total transmitted field. The total field equation for any point P outside the periodic structure is given as

#8561 - $15.00 USD Received 23 August 2005; revised 8 September 2005; accepted 12 September 2005

$$\psi(P) = \psi_{inc}(P) + \sum_{v=1}^{N} \sum_{m=-\infty}^{m=+\infty} b_{n,m} H_m^{(1)}(k_0 R_n(P)) exp(jm\theta_n(P)) \quad (7)$$

where $\psi_{inc}(P)$ is the field of an incident wave from external excitation. ψ is the electric field for TM polarization. v and N refer to the index and total number of rods. $H_m^{(1)}$ refers to the mth-order Hankel function of the first kind and k_0 is the wavenumber of incident field in vacuum. R_n and θ_n are the distance and angle of the rods with reference to a specific coordinate origin. The second term of Eq. (7) refers to the fields scattered by the individual rods, and the coefficient $b_{n,m}$ is related to the scattering or S-matrix of each individual rod, which is given as [23]

$$S_v = \begin{bmatrix} nJ'_m(k_0 r)J_m(k_0 nr) - \gamma J_m(k_0 r)J'_m(k_0 nr) \\ nH'_m(k_0 r)J_m(k_0 nr) - \gamma H_m(k_0 r)J'_m(k_0 nr) \end{bmatrix} \quad (8)$$

where γ= 1(TE), n^2(TM), and r is the radius of the rods. The scattering matrix determines the scattering amplitude of the individual rods based on the boundary conditions [21-23]. Since the rods are all identical in a PC lattice, the S-matrix is the same for all the rods, and this reduces the calculation time. The bandgap is located in the normalized frequency range a/λ between 0.274–0.429. The bandgap exists for transverse magnetic (TM) polarization where the electric field is parallel to the axis of the rods. The frequency for optical communication, 0.368, is located at the middle of the bandgap.

5. Simulation results and discussion

Figure 4 shows the propagating field distribution of the incident light through the different taper designs. Figure 5 shows normalized field intensity of the propagating wave at various positions of the linear and nonuniform PC taper waveguide. The propagating field intensity of the concave taper is increasing at a faster rate compared with the linear and convex tapers. This is due to the inward curvature of the front end of the concave taper. For the linear taper the field intensity changes linearly, due to the fixed gradient of the taper. For the convex taper, greater change in slope at the end of the taper will cause some loss. However, the coupling efficiency is not affected significantly.

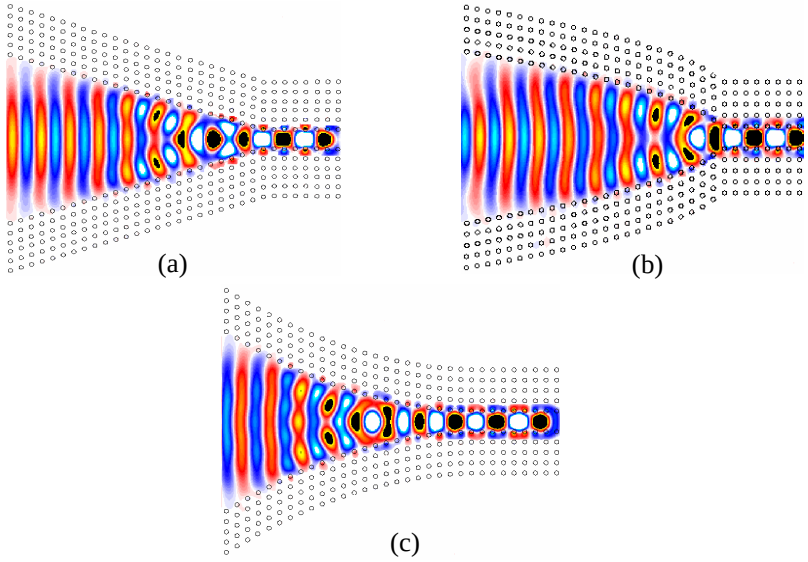

Fig. 4. Field distribution of the simulation layout: (a) linear taper; (b) convex taper; (c) concave taper.

#8561 - $15.00 USD Received 23 August 2005; revised 8 September 2005; accepted 12 September 2005

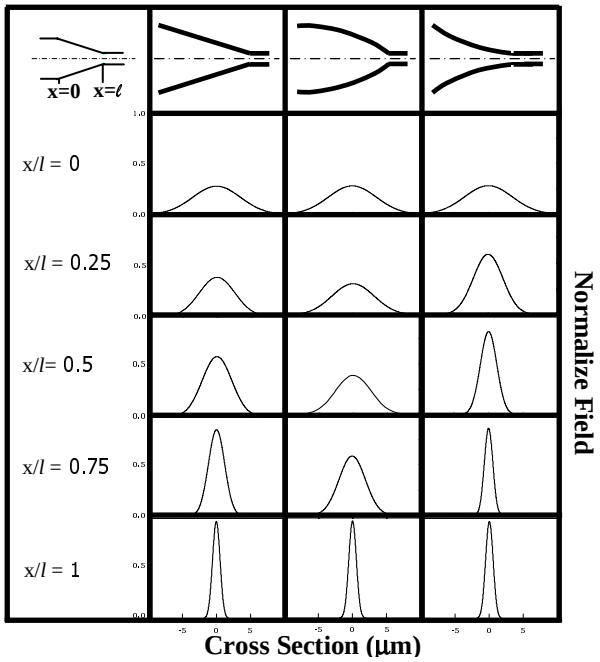

Fig. 5. Normalized field intensity of the propagating wave as a function of taper position for different taper shapes.

To show the effect of a PC taper on coupling efficiency improvement, two taper lengths at l = 9.69 μm and l = 18.24 μm are selected. Without the tapering structure, the power transmitted to the PCWG is 0.2. This is insufficient because the collected power from the output of the tapered waveguide is too weak to be of use for application to optical devices. Because of this problem, the need for a coupling taper to provide efficient modal coupling between the input light sources to the narrow PCWG is proposed. Figures 6(a) and 6(b) show the transmission spectra for a linear PC taper at l = 9.69 μm and l = 18.24 μm, respectively. In Fig. 6(a), the linear taper has an average transmittance of 0.51, whereas in Fig. 6(b) the average transmittance is 0.862 over the frequency range of 0.32–0.4. These observations tell us that modal coupling is more effective at the longer taper length because losses are reduced. At the longer taper length, the slope of taper is gentler. This means that the fundamental even mode that travels through the taper does not couple to the higher-order modes. Therefore, reflection loss is reduced and approaches the adiabatic regime. The bandpass of the spectrum at longer length has less fluctuations in comparison with the spectrum at shorter length. Two reasons can explain these fluctuations. First, the fluctuations arise because of the multiple reflections from the Fabry–Perot oscillations, which are due to the mirror cavity formed by the sides of the taper. Second, the fluctuations are observed due to the "multipath" interference caused by coupling back and forth between the multiple modes. At longer taper length, the interference and multiple reflections reduce, hence causing less fluctuation in the spectra reading and more-stable transmission spectra.

For the concave and convex PC tapers, the transmission spectra for taper with length l = 9.69 μm and l = 18.24 μm are shown in Figs. 6(c) and 6(d), respectively. In Fig. 6(c), the average transmittance of the concave taper is approximately 0.4, while for convex taper the average transmittance is 0.6. When the taper length increases to 18.24 μm, the average transmittance of the concave and the convex tapers increases to 0.8 and 0.96, respectively, for a beam reduction ratio of about 10:1. Mode-coupling efficiency of the convex taper is more effective in comparison with that of the concave taper. This is because the convex taper has a larger receiving curvature, which means that taper slope variation is more gradual in comparison with the concave taper. At the wider end of the taper, intermodal coupling is

#8561 - $15.00 USD Received 23 August 2005; revised 8 September 2005; accepted 12 September 2005

weaker, hence tapering slowly at the wider end is important for reducing the coupling to higher-order modes. This reduces reflected light as the taper becomes narrower. At the end of the convex taper, there is a little more reflection due to sharper change in the curvature that affects the overall transmittance performance only slightly. Therefore, multipath interference with input light sources for the case of the convex taper is smaller, and the band spectrum is more stable.

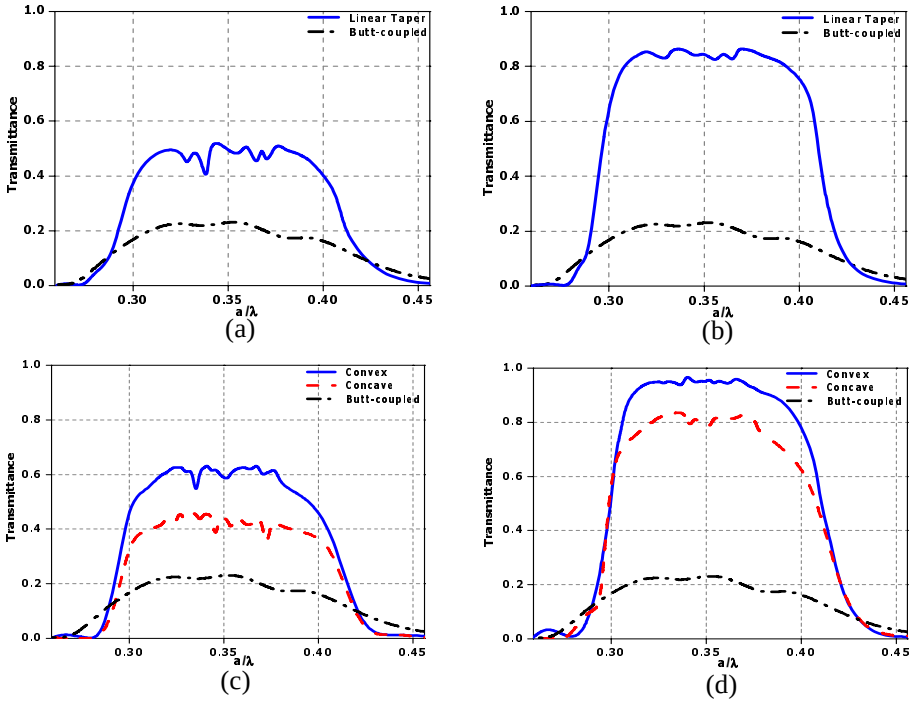

Fig. 6. Transmission spectra for the various taper shapes: (a) and (b) linear PC taper for l = 9.69 μm and 18.24 μm; (c) and (d) nonuniform PC taper l = 9.69 μm and 18.24 μm.

For the concave taper, the average transmittance also increases when the taper length increases, but the performance is less satisfactory compared with that of the convex taper. This is due to the inward curvature of the taper. The taper slope varies steeply near the front part of the taper. This variation causes the large changes in the propagation constant of the modes as the wave travels through the concave taper, resulting in higher intermodal coupling and hence reflection of light back to the fiber. There is more multipath interference and multiple reflections, which cause the transmission spectrum of the concave taper to have more ripples compared with that of the convex taper. As the taper length increases, the inward curvature of the concave taper becomes gentler. However, its coupling efficiency is still more inferior to that of the convex PC taper because the reflected waves are still relatively significant.

The power losses of the linear, concave, and convex tapers at different taper positions for lengths of 9.69 and 18.24 μm are shown in Figs. 7(a) and 7(b), respectively. These power losses include all reflection, scattering, and intermodal coupling losses. The propagation constant is calculated by supercell with the plane wave expansion method [24]. The calculation steps will not be discussed in detail, as the main objective is to introduce the loss minimization in the different taper design. For the concave taper, the sharper change in the width of the front part of the taper causes larger variation in the propagation constant of the modes, resulting in higher intermodal scattering and hence reflection losses. For the linear and convex tapers, the loss is higher at the end of the taper due to sharper change in the width of

#8561 - $15.00 USD Received 23 August 2005; revised 8 September 2005; accepted 12 September 2005

the taper. For the convex taper, the propagation constant changes more abruptly than the linear taper at the end, giving rise to higher loss value at the end of the taper.

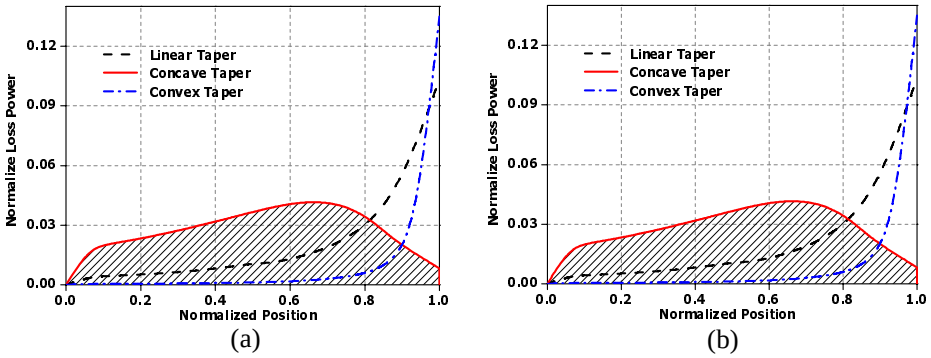

Fig. 7. Normalized loss power versus relative position for a linear taper with (a) l = 9.69 μm and (b) l = 18.24 μm. The area under the curve gives the total loss for the taper.

The area under the various curves in Figs. 7(a) and 7(b) for different taper designs can also be used to show which curvature has higher loss. From Figs. 7(a) and 7(b), the area under the concave taper is larger than that beneath the linear and convex tapers. This indicates that the concave taper suffers from higher loss. This indication indeed coincides with the observation shown in Fig 6, where the concave taper has a lower transmittance compared with the convex and linear tapers.

Next, an evaluation on the linear, concave, and convex taper designs at different taper lengths is conducted for observation of the trend of mode-coupling efficiency improvement. This is compared at a frequency of 0.368, which is the optical communication wavelength. Different values of α are substituted in Eq. (6) to show that the convex taper generally gives higher coupling efficiency compared with the linear and the concave tapers. The values of α are also varied at 1.5 and 3, as well as its reciprocal, to investigate the effect of the curvature of the nonuniform taper on coupling efficiency.

Figure 8 shows the transmittance of the linear, concave, and convex taper designs at different values of α. From Fig. 8(a), the convex taper with α values of 0.5 and 0.667 has higher transmittance than the linear taper. When α = 0.333, the transmittance is the lowest. This is because the slope of the convex taper for α = 0.333 changes even more steeply at the end of the taper. This results in more reflection and scattering losses, which reduce the coupling efficiency to a substantial amount of more than 10%.

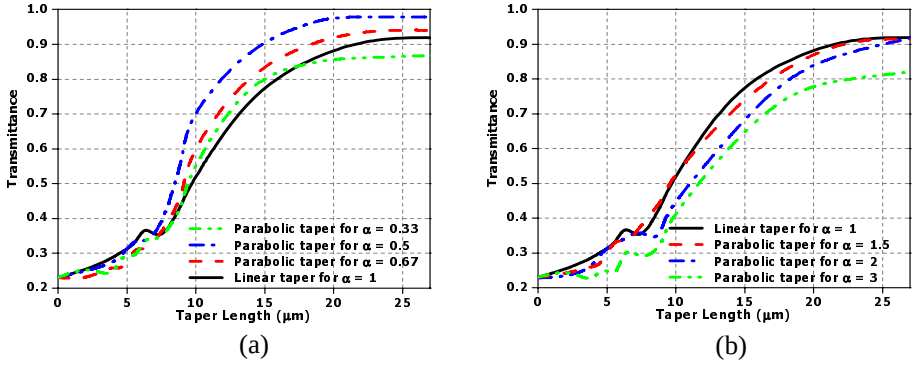

Fig. 8. Transmittance vs taper length plots for different values of α. (a) Convex shaped taper for values of α = 0.333, 0.5, 0.667. (b) Concave shaped taper for values of α = 1, 1.5, 2, 3

#8561 - $15.00 USD Received 23 August 2005; revised 8 September 2005; accepted 12 September 2005

In Fig. 8(a), the transmittance of the tapers becomes "saturated" after a certain taper length. This is because the taper has begun to experience adiabatic-like behavior. For the convex taper with $\alpha = 0.5$, the increment of the transmitted power is relatively slow after $l = 20.52$ μm. For instance, the increment is observed to be less than 0.01% for every 3 μm increase in length. Therefore, 20.52 μm is identified as the length where the transmittance of the convex taper "saturates." At this point, the taper is experiencing adiabatic mode coupling and the loss is mainly from the field pattern mismatch between the Gaussian profile input and the fundamental mode of the wide PCWG. Table 1 shows the saturation lengths and the transmittance for the different taper designs at varied lengths with different values of α. From Table 1, the saturated transmittance is 0.975 for the convex taper with $\alpha = 0.5$. This is 6% higher than that of the linear taper. Table 1 also shows that for $\alpha = 0.333$ the saturation length is shortest, but the transmittance is much lower in comparison with other values of α. Based on this comparison, it is more advisable to substitute for $\alpha = 0.5$ because the coupling is higher. This concludes that the curvature of the taper also plays an important role in determining the coupling efficiency of the nonuniform taper.

Table 1. Saturated Length and Maximum Transmittance for Different Values of α

α values	Saturated Normalized Transmittance	Saturated Length (μm)
1.000	0.912	25.080
0.333	0.862	19.950
0.500	0.975	20.520
0.667	0.934	22.810
1.500*	0.910	28.500
2.000*	0.905	28.500
3.000*	0.811	28.500

*Note: For the concave taper, the transmittance is recorded at taper length of 28.5 μm. This is the maximum taper length considered in this paper.

For the case of the concave taper, the value of α is set to be greater than 1. Generally, the mode-coupling efficiency of the concave tapers are more inferior than that of the convex and linear tapers owing to higher reflection losses. The steep taper slope has caused large variation in the propagation constant of the modes, and this results in the high intermodal scattering and coupling to higher-order modes, hence increasing reflection of incident light. When $\alpha = 3$, the inward curvature of the taper is very steep, which further leads to high back reflection. As α decreases to 2 and then 1.5, the transmittance increases as a result of the decrease in the inward curvature of the concave taper. Hence, with different values of α, the mode-conversion efficiency of the taper can be altered. The concave taper can also reach adiabatic conditions at a longer taper length than can the convex taper, because the change in the inward curvature is becoming more gradual, which in turn reduces the back reflection and multipath interference with the incident wave. In this paper, taper length is restricted at 28.5 μm, as it is not persuasive to increase mode-coupling efficiency at the expense of increasing the taper length.

From Figs. 8(a) and 8(b), it is observed that the transmittance reading does not increase smoothly but exhibits a few oscillations at the shorter lengths before it continues to increase steadily at longer lengths. This is due to the high reflection of the incident light from the PC taper. The multiple reflections and interference of the back-and-forth modes is very serious at short taper length. This causes many fluctuations in the transmission spectra, as shown in Fig. 9. The transmission spectrum is unstable for the concave PC taper at a length of about 5.7 μm. For different curvature, the amount of interference is different. For example, in the case of the

#8561 - $15.00 USD Received 23 August 2005; revised 8 September 2005; accepted 12 September 2005

concave taper, when $\alpha = 3$, there is more interference and higher back reflection. This results in more oscillations of the transmittance at the lower length.

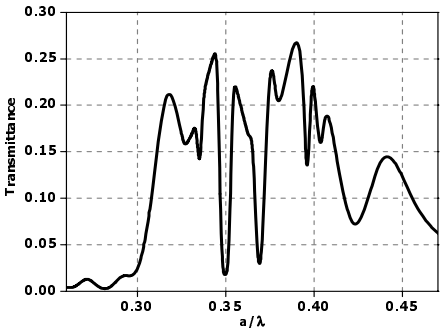

Fig. 9. Spectrum distortion for concave taper of length 5.7 μm.

6. Conclusions

In this paper, linear and nonuniform PC taper waveguides are designed and simulated. The taper has a beam reduction ratio of 10:1 for direct coupling between single-mode optical fiber and PCWG. The convex taper waveguide has a mode-conversion coupling efficiency of more than 97%. The scattering matrix method is developed for simulating the different taper designs. When $\alpha = 0.5$, the convex taper has a maximum transmittance of 0.975 at a saturated length of 20.52 μm. When $\alpha = 1$, the linear taper has a transmittance of 0.912 at a saturated length of 25.08 μm. When $\alpha = 2$, the concave taper has a transmittance of 0.918 at 25.8 μm. The convex taper has a higher transmittance of more than 6% and shorter taper length of 5 μm when compared with the linear taper. Different curvatures of taper are also simulated with various α values to compare the maximum transmittance and saturated length. In this paper, the convex taper with α values of 0.5 and 0.667 has a higher maximum transmittance and shorter length compared with the linear taper. This improvement is considered significant in terms of the mode-coupling efficiency and compactness of the taper. In addition, the study of the graph of transmittance versus taper length also shows that at shorter length, the transmittance spectrum is unstable, owing to multipath interference and Fabry–Perot reflections.

Acknowledgments

The authors express their sincerest gratitude to Steven G. Johnson of MIT for his enriching course on “photonic crystal” and his friendly advice. The authors also thank G. Tayeb of Institut Fresnel for his very useful discussion via electronic mail.